European Journal of Pharmaceutical Sciences 109 (2017) 381–388

Contents lists available at ScienceDirect

European Journal of Pharmaceutical Sciences

journal homepage: www.elsevier.com/locate/ejps

# Mannich base approach to 5-methoxyisatin 3-(4-isopropylphenyl) hydrazone: A water-soluble prodrug for a multitarget inhibition of cholinesterases, beta-amyloid fibrillization and oligomer-induced cytotoxicity

Leonardo Pisani[a], Annalisa De Palma[b], Nicola Giangregorio[c], Daniela V. Miniero[b], Paolo Pesce[a], Orazio Nicolotti[a], Francesco Campagna[a], Cosimo D. Altomare[a], Marco Catto[a,*]

[a] Dipartimento di Farmacia-Scienze del Farmaco, Università degli Studi di Bari "Aldo Moro", via E. Orabona 4, I-70125 Bari, Italy
[b] Dipartimento di Bioscienze, Biotecnologie e Biofarmaceutica, Università degli Studi di Bari "Aldo Moro", via E. Orabona 4, I-70125 Bari, Italy
[c] CNR Institute of Biomembranes, Bioenergetics and Molecular Biotechnologies, via G. Amendola 165/A, I-70126 Bari, Italy

ARTICLE INFO

*Keywords:*
Aβ oligomers
Alzheimer's disease
Indole derivatives
Multitarget inhibitors
PICUP assay

ABSTRACT

Targeting protein aggregation for the therapy of neurodegenerative diseases remains elusive for medicinal chemists, despite a number of small molecules known to interfere in amyloidogenesis, particularly of amyloid beta (Aβ) protein. Starting from previous findings in the antiaggregating activity of a class of indolin-2-ones inhibiting Aβ fibrillization, 5-methoxyisatin 3-(4-isopropylphenyl)hydrazone **1** was identified as a multitarget inhibitor of Aβ aggregation and cholinesterases with $IC_{50}$s in the low μM range. With the aim of increasing aqueous solubility, a Mannich-base functionalization led to the synthesis of *N*-methylpiperazine derivative **2**. At acidic pH, an outstanding solubility increase of **2** over the parent compound **1** was proved through a turbidimetric method. HPLC analysis revealed an improved stability of the Mannich base **2** at pH 2 along with a rapid release of **1** in human serum as well as an outstanding hydrolytic stability of the parent hydrazone. Coincubation of $Aβ_{1–42}$ with **2** resulted in the accumulation of low MW oligomers, as detected with PICUP assay. Cell assays on SH-SY5Y cells revealed that **2** exerts strong cytoprotective effects in both cell viability and radical quenching assays, mainly related to its active metabolite **1**. These findings show that **2** drives the formation of non-toxic, off-pathway Aβ oligomers unable to trigger the amyloid cascade and toxicity.

## 1. Introduction

Alzheimer's disease (AD) is the most common cause of age-related dementia. The wide increase of lifespan in developed countries shapes AD as a real epidemiologic emergency because of its high healthcare costs and the lack of disease-resolving therapies (Alzheimer's Association, 2015). As for many other neurodegenerative diseases, AD onset and progression depend on multiple causes, both genetic and sporadic, whereby the pharmacologic treatment still remains only symptomatic (Trippier et al., 2013 and Berk and Sabbagh, 2013). The histopathological hallmarks of AD are extracellular amyloid plaques, constituted by beta-amyloid (Aβ) peptide aggregates, and neurofibrillary tangles, containing microtubule-associated tau protein in a hyperphosphorylated form (Querfurth and LaFerla, 2010). Such histological features occur in specific brain areas, particularly in the basal forebrain, rich in cholinergic neurons (Terry and Buccafusco, 2003). The loss of acetylcholine (ACh) transmission is associated with the neurodegeneration, cognitive decline and mood troubles typically related to AD. In the absence of disease-modifying therapies, current pharmacological treatments of AD are mainly symptomatic and aim to restore normal ACh levels by means of acetylcholinesterase (AChE) inhibitors (Anand and Singh, 2013) or to exert neuroprotective effects throughout an *N*-methyl-D-aspartate partial antagonist, memantine (Lo and Grossberg, 2011).

One of the leading hypotheses for AD is centered on amyloidogenic aggregation of Aβ deriving from the proteolysis of amyloid precursor protein (APP) by sequential action of β- and γ-secretases (Hardy and Selkoe, 2002), that can form both 40-mer ($Aβ_{1–40}$) and the more toxic 42-mer ($Aβ_{1–42}$). Aβ peptides exist as non-fibrillar monomers, soluble oligomers, intermediate protofibrils and insoluble fibrillar aggregates (Benilova et al., 2012). It has been established that cognitive impairment and synaptic deficit in the AD brain are strongly correlated with

* Corresponding author.
*E-mail address:* marco.catto@uniba.it (M. Catto).

http://dx.doi.org/10.1016/j.ejps.2017.08.004
Received 7 April 2017; Received in revised form 13 July 2017; Accepted 7 August 2017
Available online 09 August 2017
0928-0987/ © 2017 Elsevier B.V. All rights reserved.

the neuronal toxicity of soluble oligomeric assemblies of Aβ (Benilova et al., 2012; Lambert et al., 1998; Walsh et al., 2002b; Wang et al., 2005 and Shankar et al., 2008). Building on this hypothesis, agents that prevent or reverse the oligomerization of Aβ may provide potential therapeutic application in the treatment of AD. Efforts in the search for inhibitors of Aβ aggregation have demonstrated that small molecules, containing single or multiple (hetero)aromatic rings suitably decorated, can inhibit protein-protein interactions (LeVine, 2007). Many studies suggested that the driving forces governing the Aβ assembly include aromatic packing (through π-π interactions or π-stacking), hydrophobic and electrostatic interactions between Aβ side chains (Gsponer et al., 2003; Hills and Brooks, 2007 and Paul et al., 2016). Small molecules competing with such an association could inhibit the fibrillization process (Zheng et al., 2006). Such evaluations led us to identify different chemical classes of Aβ aggregation inhibitors, particularly benzamides of glycine-based oligopeptides (Cellamare et al., 2008) and indole derivatives (Catto et al., 2010 and Campagna et al., 2011).

Increasing evidences in the pharmacological approach to AD suggest a major benefit in biasing different biological targets simultaneously, by means of a single molecular entity. Although not fully validated in therapy, such a kind of multitarget approach is indeed considered as a valuable strategy for pathologies, like AD, depending on multiple biochemical dysfunctions (Youdim and Buccafusco, 2005 and Leon et al., 2013). The advantage of single molecules acting on different targets is counteracted by the difficulty of designing such molecules that should retain multiple ligand-target affinity features and an appropriate balance of activities. This makes the multitarget ligand design a challenging task, that could be envisaged by combining ligand- and target-based drug design tools (Nicolotti et al., 2011 and Morphy and Harris, 2012).

In recent years our research group published several papers on multitarget molecules with a potential in AD treatment (Farina et al., 2015; Pisani et al. 2016a, 2016b), particularly poly(hetero)cycles with dual inhibition of cholinesterases and Aβ aggregation (Catto et al., 2012 and Tonelli et al., 2015). Among isatin-based derivatives, hit compound **1** (Campagna et al., 2011) (Scheme 1) deserved attention because of its potent anti-aggregating activity. Aiming at improving its drug-likeness profile, the aqueous solubility was preliminarily addressed. To this end, a Mannich-base approach was envisaged by preparing compound **2** from the previously published isatin, through a condensation of **1** with *N*-methylpiperazine and formaldehyde, following a reported method (Krishnan Sridhara et al., 2001). Owing to the presence of the polar and protonatable piperazine moiety, the resulting labile prodrug behaves as a water-soluble form prone to quickly release parent hydrazone **1** upon hydrolysis at pH 7.4. HPLC monitoring was undertaken to assess the conversion of compound **2** and the hydrolytic stability of compound **1**. The neuroprotective biochemical profile of **2** was assessed in vitro and in cell-based assays.

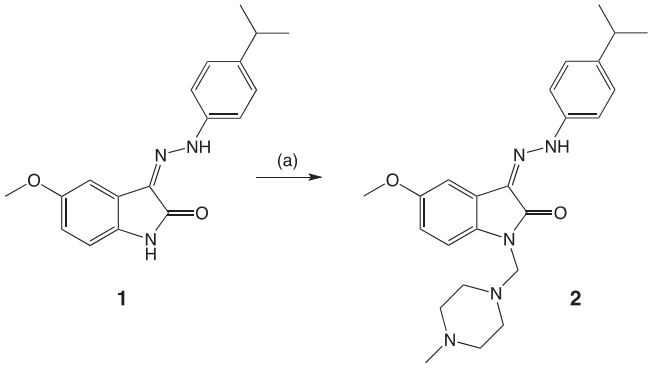


**Scheme 1.** Synthesis of compound **2**. Conditions: (a), ethyl alcohol, formaldehyde 37% wt. in water, *N*-methylpiperazine, 12 h, room temperature.

## 2. Materials and methods

### 2.1. Chemistry

Reagents and solvents were obtained from Sigma-Aldrich (Milan, Italy) and were used without further purification. All reactions were checked by TLC using Merck Kieselgel 60 $F_{254}$ aluminum plates (VWR, Milan, Italy) and visualized by UV light. The purity of all of the intermediates, checked by $^1$H NMR, was always better than 95%. Chromatographic separation was performed on Merck silica gel 63–200 (VWR, Milan, Italy), using a mixture of chloroform/methanol 90:10 (v/v) as the eluant. Melting points (mp) were determined by the capillary method on a Stuart Scientific SMP3 electrothermal apparatus (Bibby Scientific, Stone, United Kingdom) and are uncorrected. IR spectra were recorded using potassium bromide disks on a Spectrum One FT-IR spectrophotometer (Perkin Elmer, Monza, Italy); only the most significant and diagnostic absorption bands have been reported. $^1$H NMR spectra were recorded on a Mercury 300 instrument (Varian, Milan, Italy) at 300 MHz in the specified deuterated solvent. Chemical shifts ($\delta$) are quoted in parts per million (ppm) and are referenced to the residual solvent peak. The coupling constants *J* are given in Hertz (Hz). The following abbreviations were used: s (singlet), d (doublet), dd (doublet of doublets), m (multiplet), brs (broad signal); signals due to NH protons were located by deuterium exchange with $D_2O$ (exch. $D_2O$). ESI-MS was performed with an electrospray interface and an ion trap mass spectrometer (1100 Series LC/MSD Trap System Agilent, Palo Alto, CA, USA). The sample was infused via a KD Scientific syringe pump (Holliston, MA, USA) at a rate of 10 mL/min. Ionization was achieved in both positive and negative ion modes. The pressure of the nebulizer gas was 15 psi. The drying gas was heated to 350 °C at a flow of 5 L/min. Elemental analyses were performed on a EuroEA 3000 analyzer (Eurovector, Milan, Italy). The measured values for C, H and N agreed to within ± 0.40% of the theoretical values.

#### 2.1.1. (Z)-3-(2-(4-isopropylphenyl)hydrazono)-5-methoxy-1-((4-methylpiperazin-1-yl)methyl)indolin-2-one (2)

To a suspension of (Z)-3-(2-(4-isopropylphenyl)hydrazono)-5-methoxyindolin-2-one **1** (Campagna et al., 2011) (0.34 mmol, 105 mg) and formaldehyde (37% wt. aqueous solution; 1.36 mmol, 0.10 mL), a solution of *N*-methylpiperazine (1.36 mmol, 0.16 mL) in 1 mL of ethanol was added under stirring. The suspension slowly turned into a clear orange solution. After stirring overnight at room temperature, the precipitate was filtered and purified through column chromatography: 82% yield; yellow solid, mp 103–5 °C. IR ($cm^{-1}$): 2941, 2793, 1663, 1560, 1248, 1177. $^1$H NMR ($CDCl_3$) $\delta$ 1.25 (d, 6H, $J$ = 6.9 Hz), 2.26–2.28 (m, 4H), 2.43 (brs, 4H), 2.68 (brs, 4H), 3.86 (s, 3H), 4.51 (s, 2H), 6.81 (dd, 1H, $J_o$ = 8.4 Hz, $J_m$ = 2.7 Hz), 6.95 (d, 1H, $J_o$ = 8.4 Hz), 7.21–7.33 (m, 5H), 12.81 (s, 1H, exch. $D_2O$). ESI-MS m/z = 420.1 (100%) $[M - H]^-$, 444.3 (100%) $[MNa]^+$. Anal. calcd for $C_{24}H_{31}N_5O_2 \cdot H_2O$: C, 65.58; H, 7.57; N, 15.93. Found: C, 65.92; H, 7.43; N, 16.02.

### 2.2. Aqueous solubility measurement

A previously reported turbidimetric method (Pisani et al., 2016a) was used. Compounds were dissolved in DMSO (for pH 7.4: at concentrations of 1.55 and 15 mg/mL for **1**, 3 and 30 mg/mL for **2**; for pH 2.0: at concentrations of 0.15 and 3 mg/mL for **1**, 30 and 500 mg/mL for **2**) and added in portions to 50 mM Tris-HCl pH 7.4 or to 10 mM HCl, at room temperature. Increased UV absorbance was measured in the 600–800 nm range with an Agilent 8453E UV–visible spectrophotometer equipped with a cell changer. Experiments were performed in triplicates. Data are the mean ± SD.

### 2.3. Temperature coefficient measurement

$^1$H NMR spectra were recorded in DMSO-$d_6$ on a Agilent Technologies 500 apparatus (at 500 MHz) at five different temperature values (25, 35, 45, 55, 65 °C). Chemical shifts ($\delta$) are quoted in parts per million (ppm) and are referenced to the residual solvent peak. Temperature coefficient (TC) was calculated by applying the following equation:

$$TC = \Delta\delta/\Delta T$$

where $\Delta\delta$ is the difference between the NH chemical shift (ppb) at the highest (65 °C) and the lowest temperature used (25 °C), and $\Delta T$ is the variation of temperature (K). Regression analysis was performed with Prism 5.0 (GraphPad Software, La Jolla, CA, USA).

### 2.4. Reversed-phase HPLC analysis

5 or 10 µL of 10 mM stock solutions of compounds **1** and **2** in DMSO were added to 0.995 or 0.990 mL, respectively, of aqueous buffer solution (40 mM phosphate buffer, pH 7.40, 0.15 M KCl) or acidic buffer (10 mM HCl, 0.15 M KCl) or to reconstituted human serum preheated at 37 ± 0.5 °C (final compound concentrations 50 or 100 µM). Samples were kept in the dark and incubated at room temperature (25 ± 1.0 °C) or at 37 ± 0.5 °C. At appropriate time intervals, aliquots (100 µL) were taken and diluted/deproteinized with cold methanol (400 µL) before injection. In the case of serum suspensions, after the addition of methanol the samples were vortexed for 1 min and centrifuged at 3500 rpm for 5 min and the supernatant was filtered and injected. Samples were analyzed by HPLC using a Zorbax Eclypse-C18 4.6 mm × 250 mm, with 5 µm size particles on a Analytic Agilent 1260 Infinity multidetector system equipped with a 1200 series UV-diode array detector. UV spectra were recorded at 230–450 nm. Analytes were eluted in isocratic conditions by using a mixture of methanol and ammonium formate buffer (20 mM, pH 5.0), methanol/buffer 80% (v/v), as the mobile phase. The mobile phase was filtered through a Nylon-66 membrane 0.45 µm (Supelco, USA) before use. Injection volumes were 10 µL and the flow rate was 1 mL/min. Data were integrated and reported using OpenLAB software (Agilent Technologies). Calibration lines were derived by injecting 10 µL of different stock solutions of **1** or **2** (5, 10, 20, 25, 50, 100, 150 and 200 µM in methanol containing 10% DMSO, v/v) after dilution with cold methanol (100 µL to 500 µL) and measuring the peak area absorbance at 420 nm. Percentage of conversion was calculated by using the following equation:

$$\%\text{conversion} = (c_t/c_{max}) \times 100$$

where $c_t$ was the concentration measured at time t and $c_{max}$ represents the maximal concentration of **1** (equal to the initial concentration of **2** in the incubated samples at $t_0$). Each kinetic experiment was performed in triplicate. Linear and non-linear regression analyses were performed with Prism 5.0. Data are the mean ± SD.

### 2.5. ThT assay of $A\beta_{1-40}$ aggregation

Inhibition of $A\beta_{1-40}$ self-aggregation was studied by means of a spectrofluorimetric test based on thioflavin T (ThT) fluorescence, already developed and published by us (Cellamare et al., 2008) and modified as follows. $A\beta_{1-40}$ (EZBiolab, Carmel, IN, USA) was pretreated as described (Nichols et al., 2005) and dissolved to 300 µM in PBS 10 mM pH 7.4. Seven solutions (ranging from 1 to 1000 µM) of inhibitors were prepared by diluting a stock DMSO solution 1000 µM with PBS. Incubations were carried out in black round-bottomed 96-well plates (Greiner Bio-One, Kremsmünster, Austria) in triplicate for each concentration. Incubation samples were set by adding 5 µL of each $A\beta_{1-40}$ stock, inhibitor solution and 20% soln. 1,1,1,3,3,3-hexafluoro-2-propanol (HFIP; Sigma-Aldrich, Milan, Italy) in PBS, and PBS to a final volume of 50 µL. Samples devoid of inhibitor were prepared as control of the free self-aggregation. After 2 h of incubation at 25 °C, 150 µL of 25 µM ThT solution in phosphate buffer pH 6.0 were added and fluorescence read with a multiplate reader Infinite M100 Pro (Tecan, Cernusco S.N., Italy). $IC_{50}$s were determined by non-linear regression with Prism 5.0, as the mean of three independent experiments.

### 2.6. AChE and BChE inhibition

A modified protocol of Ellman's spectrophotometric assay (Catto et al., 2012 and Ellman et al., 1961), adapted to a 96-well plate procedure, was followed. Inhibition assays of AChE from electric eel (eeAChE, 463 U/mg; Sigma-Aldrich) and BChE from equine serum (esBChE, 13 U/mg; Sigma-Aldrich) were run in phosphate buffer 0.1 M, pH 8.0. Acetyl- and butyrylthiocholine iodide (Sigma-Aldrich) were used, respectively, as substrates, and 5,5′-dithiobis(2-nitrobenzoic acid) (DTNB; Sigma-Aldrich) as the chromophoric reagent. Incubations were carried out in clear flat-bottomed 96-well plates (Greiner Bio-One) in duplicate for each concentration. Seven solutions (ranging from 30 to 0.03 µM as the final concentrations) of inhibitors were prepared by diluting a stock DMSO solution 1000 µM with work buffer. Incubation samples contained 20 µL of the enzyme solution (0.9 U/mL in work buffer), 20 µL of a 3.3 mM solution of DTNB in 0.1 M phosphate buffer pH 7.0, 20 µL of a solution of the inhibitor, and 120 µL of work buffer. After incubation for 20 min at 25 °C, thiocholine substrate (20 µL of 5 mM aqueous solution) was added, and AChE-catalyzed hydrolysis was followed by measuring the increase of absorbance at 412 nm for 5 min at 25 °C in the Tecan Infinite M100 Pro multiplate reader. Inhibition values were calculated with GraphPad Prism as the mean of three independent experiments.

### 2.7. PICUP assay of $A\beta_{1-42}$ oligomerization

Samples of 50 µM $A\beta_{1-42}$ (EZBiolab), alone or in coincubation with 20 µM **2**, were prepared in PBS 10 mM pH 7.4, with 4% DMSO as the cosolvent, and incubated at 37 °C. Oligomer formation was detected using PICUP experiments as described (Rosensweig et al., 2012). Briefly, 5 µL of 1.8 mM tris(2,2-bipyridyl)dichlororuthenium(II) hexahydrate (Ru(Bpy); Sigma-Aldrich), in 10 mM sodium phosphate buffer (pH 7.4) and 5 µL of 36 mM ammonium persulfate (APS; Sigma-Aldrich), in 10 mM sodium phosphate buffer (pH 7.4) were added to 90 µL of incubation sample, and gently mixed. The solution was irradiated for 4 s with visible light using a 150-W incandescent lamp at a distance of 10 cm from the reaction sample. The reaction mixture was immediately quenched with 50 µL of Laemmli buffer (Laemmli, 1970) containing 5% β-mercaptoethanol (Sigma-Aldrich). A 35-mm single lens reflex (SLR) AE-1 Canon camera body was used with a bellows attached in place of a lens. This system provided a suitable machinery to place the sample and control its distance from the light source. The sample was illuminated through the open back of camera body using the camera shutter mechanism to control the illumination time.

### 2.8. Polyacrylamide gel electrophoresis (SDS/PAGE)

SDS/PAGE of PICUP cross-linked $A\beta_{1-42}$ samples were performed in the presence of 0.1% sodium dodecyl sulphate (SDS; Sigma-Aldrich) according to Laemmli protocol (Laemmli, 1970). A mini gel system was used. The stacking gel contained 5% acrylamide and the separating gel 15% acrylamide with an acrylamide/bisacrylamide ratio of 150. Samples were heated to 90° for 10 min. Staining was performed using a quantitative method based on a solution of 0.1% Coomassie Brilliant Blue (Sigma-Aldrich).

### 2.9. $A\beta_{1-42}$-induced neurotoxicity

SH-SY5Y cells were cultured in DMEM-Dulbecco's modified Eagle's medium (Sigma-Aldrich) supplemented with 10% (v/v) inactivated

fetal bovine serum (Sigma-Aldrich), 2 mM L-glutamine (Sigma-Aldrich), 100 μg/mL penicillin and 100 μg/mL streptomycin (Sigma-Aldrich) at 37 °C in 5% $CO_2$. For assays, the cells were grown to 70% confluence and seeded for experiment in 96-well plates at a density of 10,000 cells/well in 125 μL of cell culture medium. Experiments were performed 24 h after cells were seeded.

SH-SY5Y cell viability was determined using a conventional MTT reduction assay (Berridge and Tan, 1993). This method is based on the ability of viable cells to metabolize 3-(4,5-dimethylthiazol-2-yl)-2,5-diphenyltetrazolium bromide (MTT; Sigma-Aldrich), a water-soluble salt (yellow colour), by cellular oxidoreductase into a water-insoluble blue formazan product. Therefore, the amount of produced formazan is proportional to the viable cells. Briefly, viable cells ($10^4$/well) into 96-well cell culture plate were added with a DMEM solution of $A\beta_{1-42}$, alone or in mixture with **2** (5 μM final concentration of both) and incubated at 37 °C in 5% $CO_2$. At the end of incubation time (24 and 48 h), the culture medium was replaced by DMEM supplemented with a solution of MTT in PBS (50 μg/mL final concentration). After 2 h of incubation at 37 °C in 5% $CO_2$, this solution was removed and 200 μL of DMSO were added to each well to dissolve the product formazan.

Absorbance values were measured at 570 nm using a multilabel plate counter Victor$^3$ V (Perkin Elmer, Milan, Italy), with DMSO medium as the blank solution. The experiments, repeated twice, were carried out in sextuplicate, and the results were averaged.

### 2.10. Neurotoxicity from ROS generation

Intracellular radical oxygen species (ROS) production was evaluated using an oxidation-sensitive fluorescent probe, 2′,7′-dichlorodihydrofluorescin diacetate (DCFH-DA; Sigma-Aldrich) by slightly modifying the procedure reported by Wang and Joseph (1999). Briefly, viable SH-SY5Y cells ($10^4$/well) were seeded in a black 96-well cell culture plate for 24 h, then the cells were incubated in DMEM supplemented with different concentration (0 to 20 μM) of **2** for 1 h. After washing using PBS, DCFH-DA (50 μM final concentration) in medium without serum was added directly to each well, and the plate was incubated at 37 °C in 5% $CO_2$ for 0.5 h. After removing the medium, cells were washed twice with PBS, then 100 μM $H_2O_2$/well in DMEM was added and the cells were incubated at 37 °C in 5% $CO_2$ for an additional 30 min. The formation of fluorescent dichlorofluorescein (DCF) due to oxidation of DCFH in the presence of ROS was read directly in each well at an excitation wavelength of 485 nm and an emission wavelength of 530 nm using a multilabel plate reader Victor$^3$ V (Perkin Elmer), with DMSO medium as the control. At least three independent experiments with six replicates (n ≥ 18) were carried out, and the results were averaged.

## 3. Results and discussion

### 3.1. Solubility and hydrolytic stability

As shown in Table 1, the hydrazone compound **1** showed a low to moderate aqueous solubility moving from acidic to physiological pH (13 and 71 μM, respectively). This could be ascribed, at least in part, to the formation of a planar conformation attained by a six-membered ring stabilized by an intramolecular hydrogen bond (IMHB) between the carbonyl group and the exocyclic hydrazone NH. The presence of an IMHB usually shifts the involved proton downfield in the $^1$H NMR spectrum: this effect can be softened by increasing temperature only to a lesser extent. As temperature rises, proton exchange rate is faster. However, when an IMHB network occurs, the non-covalent cyclic arrangement is only partially weakened resulting in a smaller shielding effect. Thus, the temperature-dependent $^1$H NMR resonance frequency of exchangeable protons represents a well-established method to rapidly detect IMHB in proteins (Baxter and Williamson, 1997) and small molecules (Tardia et al., 2014). By plotting the chemical shift for the nucleus under study (i.e., exocyclic NH) as a function of the temperature, a negative slope was obtained after linear regression as displayed in Fig. 1. The effect of varying temperature produced a $\Delta\delta = -0.17$ ppm from 25 to 65 °C. A negative temperature coefficient (TC) and a small frequency shift reveals the presence of hydrogen-bonded protons as a more negative value (and slope) is usually observed for compounds unable to be stabilized by IMHB.

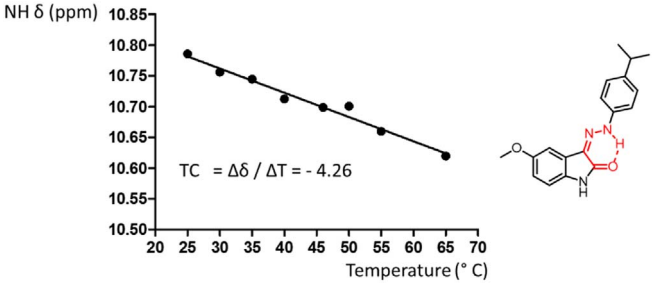


**Fig. 1.** Temperature coefficient (TC) for hydrazone NH (in red) in compound **1**. (For interpretation of the references to colour in this figure legend, the reader is referred to the web version of this article.)

A Mannich-base approach was envisaged to improve aqueous solubility and drug-like properties of **1**. Noticeably, the Mannich base **2** showed higher total solubility compared to **1** at pH 7.4 (442 vs. 71 μM), with an outstanding increase at acidic pH (17 mM vs. 13 μM; Table 1), in line with expectations. The time-course analysis of stability in the same buffer conditions used for the turbidimetric determination was performed prior to solubility measurement for compound **2**. By using 50 mM Tris buffer (pH 7.40) at room temperature, a **2**-to-**1** 50% conversion was observed after about 30 min (Fig. S1 in Supporting Informations). Solubility data refer to the sum of the species (starting Mannich base plus parent hydrazone) in conditions where degradation occurs (i.e., at physiological pH).

The stability kinetics of parent hydrazone **1** in PBS at physiological pH and temperatures of 25 and 37 °C is reported in Fig. 2A: in both cases, the hydrolytic decomposition followed a pseudo-first-order kinetics with half-lives of 71 and 24 h, respectively. By contrast, the

**Table 1**
Inhibition and solubility values of test compounds.

| Compound | $A\beta_{1-40}$ aggregation[a] | Cholinesterase inhibition[a] | | Solubility (μM) | |
|---|---|---|---|---|---|
| | | Electric eel AChE | Equine serum BChE | pH 7.4[b] | pH 2.0[c] |
| 1 | 0.43 ± 0.05[d] | 6.25 ± 0.60 | (23 ± 1%) | 71 ± 15 | 13 ± 6 |
| 2 | 1.30 ± 0.37 | 10.4 ± 0.9 | 5.43 ± 0.61 | 442 ± 16 | 17,000 ± 1900 |
| Quercetin | 0.82 ± 0.07 | nd | nd | nd | |
| Galantamine | nd | 0.51 ± 0.10 | 8.70 ± 1.02 | nd | |

[a] $IC_{50}$ (μM) or (inhibition % at 10 μM).
[b] Tris-HCl buffer.
[c] HCl 10 mM.
[d] Taken from Campagna et al., 2011.

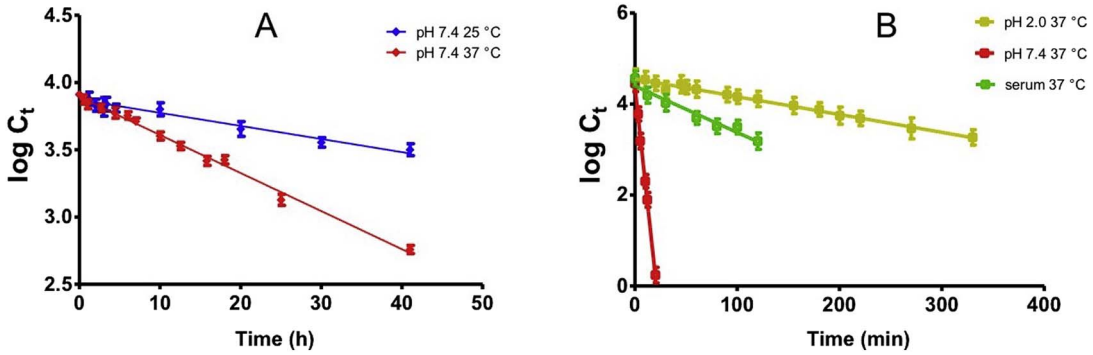


**Fig. 2.** A, time- and temperature-dependent hydrolysis of hydrazone **1** at 25 °C (blue) and 37 °C (red). B, time-dependent stability of Mannich base **2** in PBS at pH 7.4 (red), human serum (green) and at pH 2.0 (yellow) at 37 °C. $C_t$ is the concentration of compound detected at various time points, as determined by RP-HPLC. Data points represent means ± SD of three independent measurements. (For interpretation of the references to colour in this figure legend, the reader is referred to the web version of this article.)

Mannich base was labile at physiological pH, where a complete disappearance was observed within 15 min. On the other hand, the greatest stability was proved at both acidic pH and in human serum. The degradation rate followed a pseudo-first-order kinetics, with half-lives at pH 2 and in serum of 177 and 68 min, respectively (Fig. 2B), thus showing a protective effect by serum proteins.

To endorse the potential application of **2** as a prodrug of the hydrazone derivative **1**, the formation and disappearance of hydrazone **1** was monitored through a reversed-phase HPLC analysis. As shown in Fig. 3, in all cases the Mannich base **2** was converted into the parent compound **1** but with different rates. Interestingly, the highest conversion rate was observed in human serum and about 70% of the maximal hydrazone was released within 2 h. At acidic pH, where the Mannich base stability was optimal, a slow and gradual release did not exceed 20% of conversion in the same timeframe. The behavior at physiological pH reflected hydrazone and Mannich base stability time-course. Compound **2** rapidly degraded to **1**, but the hydrolytic events accelerated by temperature prevented concentration from raising. Increasing the incubation temperature in PBS from 25 to 37 °C resulted in an increase of both the release of **1** and its decomposition, as might be inferred from the linear regression obtained from the right arm of the plot in Fig. 3 (red line).

### 3.2. *In vitro and cell-based biochemical profiling*

The biochemical profile of the water-soluble Mannich base **2** was investigated in AD-related targets. The preliminary evaluation of anti-aggregating activity of **2** was achieved by means of a well-established ThT fluorescence assay (Cellamare et al., 2008), using HFIP as aggregation enhancer and PBS as incubation medium; fluorimetric

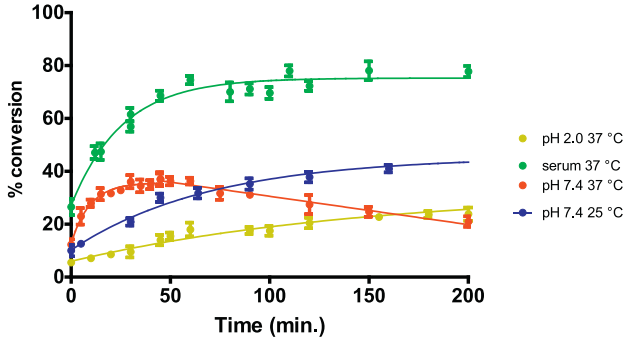


**Fig. 3.** Time- and temperature-dependent conversion of the Mannich base **2** into the parent hydrazone **1** as determined by RP-HPLC. Measurements were acquired in PBS at 25 °C (blue) and 37 °C (red), and at 37 °C in human serum (green) and HCl 10 mM (pH 2.0, yellow). Data are means ± SD of three independent experiments. (For interpretation of the references to colour in this figure legend, the reader is referred to the web version of this article.)

readings were performed after 2 h of incubation. We performed this test on $A\beta_{1-40}$ peptide, because of its less propensity to self-aggregation; in a previous work (Campagna et al., 2011) we indeed demonstrated a good superposition of inhibition data for $A\beta_{1-42}$ with those obtained from $A\beta_{1-40}$. Compounds **2** fully confirmed the good inhibition potency of its parent compound **1** (Campagna et al., 2011), with $IC_{50}$ equal to 1.30 μM (Table 1 and Fig. 4A), close to that of reference quercetin used as positive control. Taking into account the rate of hydrolysis of **2** in PBS, we can reasonably infer that the observed inhibitory effects are predominantly due to the hydrolysis product **1**, as on the other hand supported by close inhibition data ($IC_{50}$s equal 0.43 and 1.30 μM for **1** and **2**, respectively).

Inhibition assays of cholinesterases showed a weaker potency for AChE compared to galantamine, a reference drug used in the treatment of mild cognitive impairment associated to the early stage of AD (Gulcan et al., 2015). The short incubation times required for cholinesterase inhibition assay allowed a limited hydrolysis of **2**, thus leading to activity profiles well distinguishable from parent hydrazone **1**. While **1** resulted a fair and selective AChE inhibitor, compound **2** showed good inhibition of BChE, even better than galantamine, thus resulting a weakly selective BChE inhibitor (Table 1). Such activity profile is still a matter of debate concerning the usefulness of BChE inhibitors in the therapy of AD (Macdonald et al., 2014; Carotti et al., 2006 and de Candia et al., 2017); activity profiles involving selective BChE inhibition could indeed provide potential in the therapy of AD. Kinetics of BChE inhibition showed for **2** a competitive mechanism, with $K_i$ equal to 2.9 ± 0.2 μM (Fig. 4B), suggesting an interaction with the catalytic anionic site of the enzyme, in analogy with galantamine and other reversible inhibitors of ChEs.

With these evidences in hand, we proceeded with a biochemical profiling of antiaggregating activity of **2**. Our aim was to get a deeper insight into the potential of this small molecule to act as neuroprotective agent, lowering the toxicity of Aβ prefibrillar aggregates. In our previous work on the antiaggregating activity of this class of compounds (Campagna et al., 2011), we assessed their inhibitory profile by means of electron microscopy (EM) and dynamic light scattering (DLS). This study demonstrated that 3-arylhydrazonoindolin-2-one derivatives, including compound **1**, interfere with the $A\beta_{1-40}$ aggregation pathway by stabilizing the prefibrillar aggregates and inhibiting the onset of detectable fibrillar species. Prefibrillar aggregates consist in oligomers of Aβ (from 2-mers to 18-mer) (Bernstein et al., 2009 and Larson and Lesné, 2012) that are considered mostly responsible for neurotoxicity and neuronal damage in AD (Walsh et al., 2002a). In this respect, the accumulation of oligomers induced by an inhibitor of fibrillization would result ineffectual and even harmful. To face this issue, we investigated the pattern of prefibrillar aggregates, formed by the highly in vivo toxic $A\beta_{1-42}$ in the presence of inhibitor, by means of photo-induced cross-linking of unmodified protein (PICUP), a technique orthogonal to EM and DLS. PICUP allows detecting low molecular

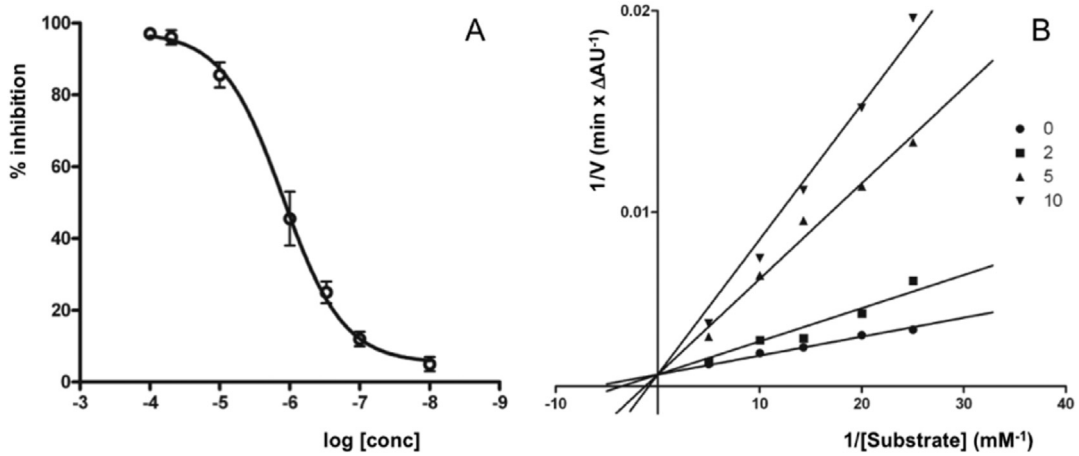


**Fig. 4.** A, dose-response curve of inhibition of $A\beta_{1-40}$ aggregation by **2**. B, Lineweaver-Burk plot of inhibition kinetics of **2** on equine serum BChE (inset: inhibitor concentrations, μM).

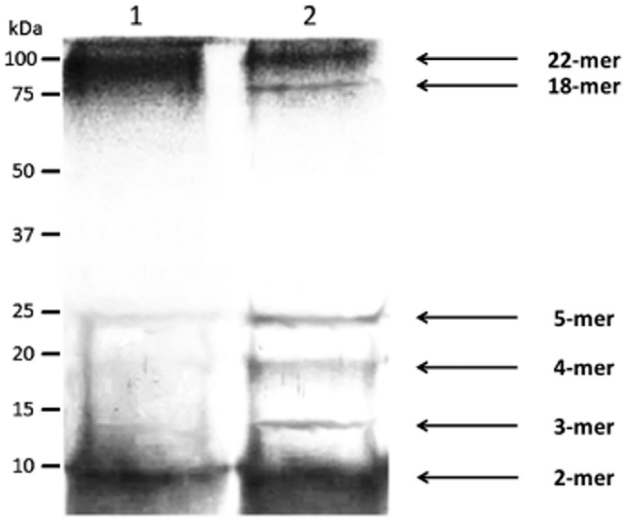


**Fig. 5.** PICUP results. $A\beta_{1-42}$ was cross-linked after incubation at 37 °C for 24 h in absence (lane 1) and in presence of **2** (lane 2) and analyzed by SDS-PAGE/Coomassie blue staining. The gel is representative of those obtained in three independent experiments.

weight (MW) oligomers of aggregating proteins by freezing their actual association through the formation of covalent interchain bonds, induced by photolysis of a tris-bipyridyl Ru(II) complex (Bitan et al., 2001 and Bitan, 2006). It could be considered as an investigational tool able to overcome the limited structural information on oligomeric assemblies brought by DLS and EM, ultimately providing useful information only for high MW species. Samples of incubation of 50 μM $A\beta_{1-42}$, alone or in the presence of 20 μM **2**, were collected at 24 h and cross-linked to generate covalently linked oligomers, detected by SDS-PAGE electrophoresis (Fig. 5). Again, this long incubation time would warrant a complete hydrolysis of **2** to **1**, making us confident that **1** was the true inhibitory species in this assay. In the free incubation sample (lane 1), a large amount of high MW species (> 80 kDa) was related to an advanced aggregated state to > 20-mers, while the presence of dimers was still detectable. Densitometric evaluation accounted for ca. 50% of high MW species and 40% of dimer, with a very residual amount of oligomers with intermediate MW. Such features were in agreement with literature evidences (Catto et al., 2012 and Feng et al., 2009) and correlated well with the high propensity of $A\beta_{1-42}$ to aggregate in vitro in physiological-mimicking conditions, giving high MW species readily detectable by means of DLS and EM (Bitan et al., 2003).

Samples coincubated with **2** showed a quite different profile of oligomer population (Fig. 5, lane 2). The marked decrease of high MW species to ca. 20% was accompanied with the appearance of a band of 18-mer (10%) and three bands, accounting for an overall 30% of densitometric measure, and amenable to intermediate 3- to 5-mers. The remaining 40% of peptide was still present as dimer. Such evidence confirmed our previous results (Campagna et al., 2011 and Catto et al., 2014), demonstrating for **2** the inhibition of fibrillization process through the accumulation of intermediate low MW species (dimers to pentamers) sparsely detectable in the free incubation sample of $A\beta_{1-42}$.

The evidence of the accumulation of non-toxic low MW oligomers was confirmed by the results of cytotoxicity assay on SH-SY5Y human neuroblastoma cells, in a conventional 3-(4,5-dimethylthiazol-2-yl)-2,5-diphenyltetrazolium bromide (MTT)-based assay. A net cytoprotective effect towards $A\beta_{1-42}$-induced cellular death was obtained with equimolar concentrations of **2** either after 24 and 48 h of coincubation, compared with untreated cells (Fig. 6A). This evidence, in accordance with our previous results (Catto et al., 2014), suggests a cytoprotective effect related not only to the disruption of the amyloidogenesis, but also operating through different cellular pathways. In this light we performed a cellular assay on SH-SY5Y cells coincubated with **2** in the presence of 2′,7′-dichlorodihydrofluorescin diacetate (DCFH-DA), a fluorescent probe of reactive oxygen species (ROS) production, to disclose possible antioxidant properties for **2**. Fig. 6B displays a strong reduction of intracellular ROS in $H_2O_2$ treated cells at concentrations of **2** equal or higher than 5 μM. Consequently, our indolinone derivative shares neuroprotective features similar to resveratrol (Feng et al., 2009) and epigallocatechine gallate (Ehrnhoefer et al., 2008), two potential neuroprotective agents. Besides the well-known antioxidant properties of arylhydrazones, it could be a matter of investigation that the 5-methoxy substituent on the isatin scaffold may undergo a metabolic demethylation in vivo, affording the formation of a 5-hydroxyindole metabolite, which is a well-known antioxidant and neuroprotective moiety (Cadenas et al., 1989).

## 4. Conclusions

Targeting protein-protein aggregation in neurodegenerative diseases remains an outstanding research topic, yet being still elusive in view of therapeutic intervention (Eisele et al., 2015). Herein we developed a Mannich-base precursor of the hydrazone compound **1**, whose potential is rooted on the multitarget activity as Aβ aggregation and cholinesterase inhibitor, ROS scavenger and neuroprotective agent against cellular damage induced by $A\beta_{1-42}$. Solubility and stability studies proved the potential of the Mannich base approach to provide water-soluble and labile prodrugs, suggesting a possible good bioavailability after oral administration. In fact, the Mannich base displayed a high solubility along with a good hydrolytic stability in acidic medium (pH 2, high ionic strength) similar to that of the gastric fluid. In addition, it allowed a fast and efficient release in human serum of the

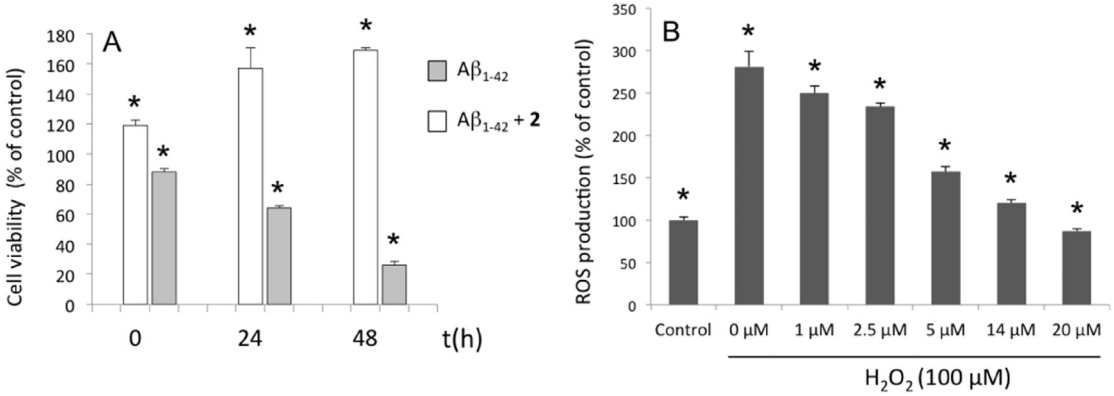


**Fig. 6.** A, effects of **2** on SH-SY5Y cell viability measured by the MTT assay, after 0, 24, 48 h of incubation at 37 °C of $A\beta_{1-42}$ 5 μM, in the absence (grey bars) and presence (white bars) of 5 μM **2**. The percentage of MTT reduction is relative to control cells (DMEM). B, effects of **2** on intracellular ROS production in DCFH-DA assay. SH-SY5Y cells were treated with different concentrations of **2** (0–20 μM) prior to $H_2O_2$ (100 μM) exposure. The percentage of ROS production in the presence of **2** is relative to control cells (DMEM). Values are expressed as mean ± SEM from six replicates, significantly different from the respective control as estimated by the Student's *t*-test (*$p < 0.01$).

parent hydrazone compound. Combining PICUP and cell assays, we outlined the neuroprotection exerted by **2** in forming non-toxic, off-pathway low MW oligomers. Such neuroprotective effect was also well correlated with the radical scavenging properties. Additionally, the increase of cholinergic function warranted by BChE and, to a less extent, AChE inhibition could be useful against memory impairment typical of AD, deserving further investigations in animal models of AD.

Supplementary data to this article can be found online at http://dx.doi.org/10.1016/j.ejps.2017.08.004.

## Acknowledgments

Financial support was warranted by University of Bari "Aldo Moro" (GRBA11EB3G) (Progetto IDEA Giovani Ricercatori 2012). L. Pisani acknowledges financial support from APQ Research Apulian Region "FutureInResearch" (FKY7YJ5) - Regional program for smart specialization and social and environmental sustainability - Fondo di Sviluppo e Coesione 2007-2013.

## References

Alzheimer's Association, 2015. 2015 Alzheimer's disease facts and figures. Alzheimers Dement. 11, 332–384.
Anand, P., Singh, B., 2013. A review on cholinesterase inhibitors for Alzheimer's disease. Arch. Pharm. Res. 36, 375–399.
Baxter, N.J., Williamson, M.P., 1997. Temperature dependence of 1H chemical shifts in proteins. J. Biomol. NMR 9, 359–369.
Benilova, I., Karran, E., De Strooper, B., 2012. The toxic Aβ oligomer and Alzheimer's disease: an emperor in need of clothes. Nat. Neurosci. 15, 349–357.
Berk, C., Sabbagh, M.N., 2013. Successes and failures for drugs in late-stage development for Alzheimer's disease. Drugs Aging 10, 783–792.
Bernstein, S.L., Dupuis, N.F., Lazo, N.D., Wyttenbach, T., Condron, M.M., Bitan, G., Teplow, D.B., Shea, J.E., Ruotolo, B.T., Robinson, C.V., Bowers, M.T., 2009. Amyloid-β protein oligomerization and the importance of tetramers and dodecamers in the aetiology of Alzheimer's disease. Nat. Chem. 1, 326–331.
Berridge, M.V., Tan, A.S., 1993. Characterization of the cellular reduction of 3-(4,5-dimethylthiazol-2-yl)-2,5-diphenyltetrazolium bromide (MTT): subcellular localization, substrate dependence, and involvement of mitochondrial electron transport in MTT reduction. Arch. Biochem. Biophys. 303, 474–482.
Bitan, G., 2006. Structural study of metastable amyloidogenic protein oligomers by photo-induced cross-linking of unmodified proteins. Methods Enzymol. 413, 217–236.
Bitan, G., Lomakin, A., Teplow, D.B., 2001. Amyloid beta-protein oligomerization: prenucleation interactions revealed by photo-induced cross-linking of unmodified proteins. J. Biol. Chem. 276, 35176–35184.
Bitan, G., Kirkitadze, M.D., Lomakin, A., Vollers, S.S., Benedek, G.B., Teplow, D.B., 2003. Amyloid beta-protein (Abeta) assembly: Abeta 40 and Abeta 42 oligomerize through distinct pathways. Proc. Natl. Acad. Sci. U. S. A. 100, 330–335.
Cadenas, E., Simic, M.G., Sies, H., 1989. Antioxidant activity of 5-hydroxytryptophan, 5-hydroxyindole, and DOPA against microsomal lipid peroxidation and its dependence on vitamin E. Free Radic. Res. Commun. 6, 11–17.
Campagna, F., Catto, M., Purgatorio, R., Altomare, C.D., Carotti, A., De Stradis, A., Palazzo, G., 2011. Synthesis and biophysical evaluation of arylhydrazono-1H-2-indolinones as β-amyloid aggregation inhibitors. Eur. J. Med. Chem. 46, 275–284.
Carotti, A., de Candia, M., Catto, M., Borisova, T.N., Varlamov, A.V., Méndez-Álvarez, E., Soto-Otero, R., Voskressensky, L.G., Altomare, C.D., 2006. Ester derivatives of annulated tetrahydroazocines: a new class of selective acetylcholinesterase inhibitors. Bioorg. Med. Chem. 14, 7205–7212.
Catto, M., Aliano, R., Carotti, A., Cellamare, S., Palluotto, F., Purgatorio, R., De Stradis, A., Campagna, F., 2010. Design, synthesis and biological evaluation of indane-2-arylhydrazinylmethylene-1,3-diones and indol-2-aryldiazenylmethylene-3-ones as beta-amyloid aggregation inhibitors. Eur. J. Med. Chem. 45, 1359–1366.
Catto, M., Berezin, A.A., Lo Re, D., Loizou, G., Demetriades, M., De Stradis, A., Campagna, F., Koutentis, P.A., Carotti, A., 2012. Design, synthesis and biological evaluation of benzo[e][1,2,4]triazin-7(1H)-one and [1,2,4]-triazino[5,6,1-jk]carbazol-6-one derivatives as dual inhibitors of beta-amyloid aggregation and acetyl/butyryl cholinesterase. Eur. J. Med. Chem. 58, 84–97.
Catto, M., Arnesano, F., Palazzo, G., De Stradis, A., Calò, V., Losacco, M., Purgatorio, R., Campagna, F., 2014. Investigation on the influence of (Z)-3-(2-(3-chlorophenyl)hydrazono)-5,6-dihydroxyindolin-2-one (PT2) on β-amyloid(1-40) aggregation and toxicity. Arch. Biochem. Biophys. 560, 73–82.
Cellamare, S., Stefanachi, A., Stolfa, D.A., Basile, T., Catto, M., Campagna, F., Sotelo, E., Acquafredda, P., Carotti, A., 2008. Design, synthesis, and biological evaluation of glycine-based molecular tongs as inhibitors of Abeta1-40 aggregation in vitro. Bioorg. Med. Chem. 16, 4810–4822.
De Candia, M., Zaetta, G., Denora, N., Tricarico, D., Majellaro, M., Cellamare, S., Altomare, C.D., 2017. New azepino[4,3-b]indole derivatives as nanomolar selective inhibitors of human butyrylcholinesterase showing protective effects against NMDA-induced neurotoxicity. Eur. J. Med. Chem. 125, 288–298.
Ehrnhoefer, D.E., Bieschke, J., Boeddrich, A., Herbst, M., Masino, L., Lurz, R., Engemann, S., Pastore, A., Wanker, E.E., 2008. EGCG redirects amyloidogenic polypeptides into unstructured, off-pathway oligomers. Nat. Struct. Mol. Biol. 15, 558–566.
Eisele, Y.S., Monteiro, C., Fearns, C., Encalada, S.E., Wiseman, R.L., Powers, E.T., Kelly, J.W., 2015. Targeting protein aggregation for the treatment of degenerative diseases. Nat. Rev. Drug Discov. 14, 759–780.
Ellman, G.L., Courtney, K.D., Andres Jr., V., Featherstone, R.M., 1961. A new and rapid colorimetric determination of acetylcholinesterase activity. Biochem. Pharmacol. 7, 88–95.
Farina, R., Pisani, L., Catto, M., Nicolotti, O., Gadaleta, D., Denora, N., Soto-Otero, R., Mendez-Alvarez, E., Passos, C.S., Muncipinto, G., Altomare, C.D., Nurisso, A., Carrupt, P.A., Carotti, A., 2015. Structure-based design and optimization of multi-target-directed 2H-chromen-2-one derivatives as potent inhibitors of monoamine oxidase B and cholinesterases. J. Med. Chem. 58, 5561–5578.
Feng, Y., Wang, X.P., Yang, S.G., Wang, Y.J., Zhang, X., Du, X.T., Sun, X.X., Zhao, M., Huang, L., Liu, R.T., 2009. Resveratrol inhibits beta-amyloid oligomeric cytotoxicity but does not prevent oligomer formation. Neurotoxicology 30, 986–995.
Gsponer, J., Haberthur, U., Caflisch, A., 2003. The role of side-chain interactions in the early steps of aggregation: molecular dynamics simulations of an amyloid-forming peptide from the yeast prion Sup35. Proc. Natl. Acad. Sci. U. S. A. 100, 5154–5159.
Gulcan, H.O., Orhan, I.E., Sener, B., 2015. Chemical and molecular aspects on interactions of galantamine and its derivatives with cholinesterases. Curr. Pharm. Biotechnol. 16, 252–258.
Hardy, J., Selkoe, D.J., 2002. The amyloid hypothesis of Alzheimer's disease: progress and problems on the road to therapeutics. Science 297, 353–356.
Hills Jr., R.D., Brooks 3rd., C.L., 2007. Hydrophobic cooperativity as a mechanism for amyloid nucleation. J. Mol. Biol. 368, 894–901.
Krishnan Sridhara, S.K., Saravanana, M., Ramesh, A., 2001. Synthesis and antibacterial screening of hydrazones, Schiff and Mannich bases of isatin derivatives. Eur. J. Med. Chem. 36, 615–625.
Laemmli, U.K., 1970. Cleavage of structural proteins during the assembly of the head of bacteriophage T4. Nature 227, 680–685.
Lambert, M.P., Barlow, A.K., Chromy, B.A., Edwards, C., Freed, R., Liosatos, M., Morgan, T.E., Rozovsky, I., Trommer, B., Viola, K.L., Wals, P., Zhang, C., Finch, C.E., Krafft, G.A., Klein, W.L., 1998. Diffusible, nonfibrillar ligands derived from Abeta1-42 are potent central nervous system neurotoxins. Proc. Natl. Acad. Sci. U. S. A. 95,

6448–6453.
Larson, M.E., Lesné, S.E., 2012. Soluble Aβ oligomer production and toxicity. J. Neurochem. 120, 125–139.
Leon, R., Garcia, A.G., Marco-Contelles, J., 2013. Recent advances in the multitarget-directed ligands approach for the treatment of Alzheimer's disease. Med. Res. Rev. 33, 139–189.
LeVine 3rd., H., 2007. Small molecule inhibitors of Abeta assembly. Amyloid 14, 185–197.
Lo, D., Grossberg, G.T., 2011. Use of memantine for the treatment of dementia. Expert. Rev. Neurother. 11, 1359–1370.
Macdonald, I.R., Rockwood, K., Martin, E., Darvesh, S., 2014. Cholinesterase inhibition in Alzheimer's disease: is specificity the answer? J. Alzheimers Dis. 42, 379–384.
Morphy, J.R., Harris, C.J. (Eds.), 2012. Designing Multi-Target Drugs. RSC Publishing, London.
Nichols, M.R., Moss, M.A., Reed, D.K., Cratic-McDaniel, S., Hoh, J.H., Rosenberry, T.L., 2005. Amyloid-beta protofibrils differ from amyloid-beta aggregates induced in dilute hexafluoroisopropanol in stability and morphology. J. Biol. Chem. 280, 2471–2480.
Nicolotti, O., Giangreco, I., Introcaso, A., Leonetti, F., Stefanachi, A., Carotti, A., 2011. Strategies of multi-objective optimization in drug discovery and development. Expert Opin. Drug Discovery 6, 871–884.
Paul, A., Sharma, B., Mondal, T., Thalluri, K., Paul, S., Mandal, B., 2016. Amyloid β derived switch-peptides as a tool for investigation of early events of aggregation: a combined experimental and theoretical approach. Med. Chem. Commun. 7, 311–316.
Pisani, L., Farina, R., Catto, M., Iacobazzi, R., Nicolotti, O., Cellamare, S., Mangiatordi, G.F., Denora, N., Soto-Otero, R., Siragusa, L., Altomare, C.D., Carotti, A., 2016a. Exploring basic tail modifications of coumarin-based dual acetylcholinesterase-monoamine oxidase B inhibitors: identification of water-soluble, brain-permeant neuroprotective multitarget agents. J. Med. Chem. 59, 6791–6806.
Pisani, L., Farina, R., Soto-Otero, R., Denora, N., Mangiatordi, G.F., Nicolotti, O., Mendez-Alvarez, E., Altomare, C.D., Catto, M., Carotti, A., 2016b. Searching for multi-targeting neurotherapeutics against Alzheimer's: discovery of potent AChE-MAO B inhibitors through the decoration of the 2H-chromen-2-one structural motif. Molecules 21, 362–376.
Querfurth, H.W., LaFerla, F.M., 2010. Alzheimer's disease. N. Engl. J. Med. 362, 329–344.
Rosensweig, C., Ono, K., Murakami, K., Lowenstein, D.K., Bitan, G., Teplow, D.B., 2012. Preparation of stable amyloid β-protein oligomers of defined assembly order. Methods Mol. Biol. 849, 23–31.
Shankar, G.M., Li, S., Mehta, T.H., Garcia-Munoz, A., Shepardson, N.E., Smith, I., Brett, F.M., Farrell, M.A., Rowan, M.J., Lemere, C.A., Regan, C.M., Walsh, D.M., Sabatini, B.L., Selkoe, D.J., 2008. Amyloid-beta protein dimers isolated directly from Alzheimer's brains impair synaptic plasticity and memory. Nat. Med. 14, 837–842.
Tardia, P., Stefanachi, A., Niso, M., Stolfa, D.A., Mangiatordi, G.F., Alberga, D., Nicolotti, O., Lattanzi, G., Carotti, A., Leonetti, F., Perrone, R., Berardi, F., Azzariti, A., Colabufo, N.A., Cellamare, S., 2014. Trimethoxybenzanilide-based P-glycoprotein modulators: an interesting case of lipophilicity tuning by intramolecular hydrogen bonding. J. Med. Chem. 57, 6403–6418.
Terry, A.V., Buccafusco, J.J., 2003. The cholinergic hypothesis of age and Alzheimer's disease-related cognitive deficits: recent challenges and their implications for novel drug development. J. Pharmacol. Exp. Ther. 306, 821–882.
Tonelli, M., Catto, M., Tasso, B., Novelli, F., Canu, C., Iusco, G., Pisani, L., De Stradis, A., Denora, N., Sparatore, A., Boido, V., Carotti, A., Sparatore, F., 2015. Multitarget therapeutic leads for Alzheimer's disease: quinolizidinyl derivatives of bi- and tricyclic systems as dual inhibitors of cholinesterases and β-amyloid (Aβ) aggregation. ChemMedChem 10, 1040–1053.
Trippier, P.C., Labby, K.J., Hawker, D.D., Mataka, J., Silverman, R.B., 2013. Target- and mechanism-based therapeutics for neurodegenerative diseases: strength in numbers. J. Med. Chem. 56, 3121–3147.
Walsh, D.M., Klyubin, I., Fadeeva, J.V., Cullen, W.K., Anwyl, R., Wolfe, M.S., Rowan, M.J., Selkoe, D.J., 2002a. Naturally secreted oligomers of amyloid beta protein potently inhibit hippocampal long-term potentiation in vivo. Nature 416, 535–539.
Walsh, D.M., Klyubin, I., Fadeeva, J.V., Rowan, M.J., Selkoe, D.J., 2002b. Amyloid-β oligomers: their production, toxicity and therapeutic inhibition. Biochem. Soc. Trans. 30, 552–557.
Wang, H., Joseph, J.A., 1999. Quantifying cellular oxidative stress by dichlorofluorescein assay using microplate reader. Free Radic. Biol. Med. 27, 612–616.
Wang, H., Pasternak, J.F., Kuo, H., Ristic, H., Lambert, M.P., Chromy, B., Viola, K.L., Klein, W.L., Stine, W.B., Krafft, G.A., Trommer, B.L., 2005. Soluble oligomers of β amyloid (1-42) inhibit long-term potentiation but not long-term depression in rat dentate gyrus. Brain Res. 924, 133–140.
Youdim, M.B., Buccafusco, J.J., 2005. CNS targets for multifunctional drugs in the treatment of Alzheimer's and Parkinson's diseases. J. Neural Transm. 112, 519–537.
Zheng, J., Ma, B., Nussinov, R., 2006. Consensus features in amyloid fibrils: sheet-sheet recognition via a (polar or nonpolar) zipper structure. Phys. Biol. 3, 1–4.